Magnetorheological Polishing Based on Honing Vertical Mechanism for Inner Surface of Titanium Alloy Pipes

Wanli Song *, Zhen Yang , Dezhi Meng , Na Wang , Seung-Bok Choi *

Posted Date: 7 February 2024

doi: 10.20944/preprints202402.0423.v1

Keywords: magnetorheological polishing fluid; vertical magnetorheological polishing; internal surface; simulation analysis; surface roughness

Article

Magnetorheological Polishing Based on Honing Vertical Mechanism for Inner Surface of Titanium Alloy Pipes

Wanli Song [1,*], Zhen Yang [1], Dezhi Meng [1], Na Wang [1] and Seung-Bok Choi [2,3,*]

[1] School of Mechanical Engineering and Automation, Northeastern University, Shenyang, 110819, China; songwl@me.neu.edu.cn; 496854468@qq.com; 2751308923@qq.com; wangn@me.neu.edu.cn

[2] Department of Mechanical Engineering, The State University of New York, Korea (SUNY Korea), Incheon 21985, Korea; seungbok.choi@sunykorea.ac.kr

[3] Department of Mechanical Engineering, Industrial University of Ho Chi Minh City (IUH), Ho Chi Minh City 70000, Vietnam

* Correspondence: songwl@me.neu.edu.cn; seungbok.choi@sunykorea.ac.kr

Abstract: Recently, a high internal surface of the titanium alloy pipe is required due to the increment of various applications of the pipe such as aerospace. However, the traditional machining process is unable to effectively polish the internal surface of the slender pipe. Thus, a vertical magnetorheological polishing (VMRP) apparatus is carried out in this work to implement high polishing performance on the internal surface of the titanium alloy pipe. The polishing process is realized by the combination of the rotating motion of the pipe and the reciprocating linear motion of the polishing head. Moreover, a series of comparative experiments are conducted to investigate the polishing mechanism of magnetorheological (MR) fluid and enhance the polishing performance. It is shown from the experimental results that proposed VMRP approach exhibits the better polishing performance than the conventional horizontal MR polishing method under same testing conditions. This is because the proposed VMRP method well eliminates the traces of polishing particles owing to the combination of polishing particles with different sizes. In addition, it is identified from the experimental test that the polishing time of the VMRP required to achieve the same polishing effect as the conventional method is shortened under the combination of different rotation speeds. It is identified from the above benefits of the VMRP that the final surface roughness after polishing is below 0.05 μm.

Keywords: magnetorheological polishing fluid; vertical magnetorheological polishing; internal surface; simulation analysis; surface roughness

1. Introduction

Titanium alloy is widely used in the field of machine manufacturing. In the aviation and aerospace industry, titanium alloy is one of the main materials of modern aircraft and engines due to its low density, high specific strength, superior corrosion resistance, and good process performance [1]. High-quality titanium alloys can operate for a long time at a temperature above 600℃, which is mainly used in manufacturing supersonic fighter aircraft, compressors blades, housing and casing parts of fans, and turbine disks of jet engines [2]. Moreover, the amount of titanium alloy used in modern aircraft has reached 30%-50% of the weight of the entire structure. For example, the use of titanium alloy in F-22 fighter jets reaches 41% [3]. The titanium-alloy pipe is widely used in the aerospace industry, and its internal surface is required to have a high surface finish because of the high demand for fuel transportation pipelines for flow. Hence, the internal surface of the titanium-alloy pipe needs to be polished to improve the surface roughness and eliminate surface defects. However, it is difficult to process the internal surface of titanium-alloy pipes because of the low thermal conductivity, high strength at elevated temperatures, and high chemical reactivity [4,5]. Titanium alloy cannot be effectively polished by the traditional machining process, and the labor intensity is high [6]. Magnetorheological (MR) polishing can accurately control the polishing process on complex surfaces because of the rheological properties of MR fluid by an external magnetic field

 doi:10.20944/preprints202402.0423.v1

or current [7–9]. Therefore, MR polishing method is adopted to address these problems encountered when polishing the internal surface of titanium-alloy pipes.

The technology of MR polishing has been intensively investigated in last three decades. In the 1980s, Japanese scholars proposed introducing a magnetic field into optical material processing [10]. Then, after 1990s, Kordonski and his team put forward the MR polishing technology. They cooperated with QED Company to manufacture a general MR polishing test machine, which successfully realized the commercialization of MR polishing technology [11,12]. The rotating tool MR fluid method is the optimal choice for the polishing of the internal surface of the titanium-alloy pipe. In general, the typical rotating finishing tool consists of the ball end and flexible ball-shaped finishing tool. The tool is made to be stiff to resist MR polishing fluid under the high magnetic field, which is capable to polish the complex surfaces such concave, convex, aspheric, and 3D surfaces, and overcomes the shape limitations of magnetic field-assisted finishing processes because of the movement flexibility of the ball end MR polishing tool to the workpiece surface [13–15]. Jung et al used sintered iron carbon nano-pipes as new magnetic abrasive particles in the MR finishing process for hard materials [16]. The removal efficiency of the surface material can be enhanced by sintering the magnetic abrasive particles and polishing particles together. Barman and Das [17] proposed a chemical assisted magnetic field polishing method of titanium-alloy, using MR finishing as the polishing fluid to achieve the polishing of titanium alloy. After polishing, the surface roughness of the titanium-alloy workpiece had reached nanoscale, but this chemical operation method was complicated, and the chemical substances used were dangerous. Laser-assisted machining and ultrasonic vibration-assisted machining have been both demonstrated to enhance the machinability of the titanium alloy, but much further work is required to better implement these technologies [18]. Kumar et al made an experiment on machining of Ti-6Al-4V by using electro discharge machining and took pulse on time, voltage and current as the machined parameters. The experiment shows that material removal rate and surface roughness were directly proportional to discharge current and utilized for optimization of process variables [19].

For the polishing of internal surface of pipe fittings, Wang et al [20] designed a variety of pole arrangement schemes along the circumference of the pipe for polishing the internal surface of slender austenitic stainless steel pipe fittings with magnetic abrasive. Under the N-S-S-N layout, the effects of rotation speed, polishing time, and magnetic field strength on the polishing effect were studied, but the polishing mechanism was not analyzed in detail, and the internal surface topography before and after polishing was not shown. Zou and Shinmura [21] polished the internal surface of 304 stainless steel pipe fittings and enhanced the magnetic field strength and polishing effect through the combination of the internal magnetic pole and the external magnetic pole. However, this magnetic field arrangement resulted in a large volume of embedded excitation device, which was only suitable for pipe fittings with large internal diameter. Kang et al [22], for the ultra-fine short pipe, used the heat-treated magnetic workpiece, arranged multiple magnetic poles on the single direction moving guide rail to achieve simultaneous polishing of multiple areas and improve the polishing efficiency. The polishing particles at the highest speed can still keep stable and have good polishing performance in the single pole polishing. However, in the process of multipole polishing, the abrasive particles and workpiece are unstable due to the high centrifugal force, resulting in deep scratches and irregular defects on the machined surface. Sadiq and Shunmugam [23] designed MR abrasive flow honing device. The influence of the sample's magnetic conductivity on the polishing effect and the influence of the magnetic material on the polishing effect by changing the magnetic field distribution were studied. It was confirmed that the polishing effect could be enhanced by changing the magnetic field distribution by placing magnetic materials on the shaft. Grover and Singh [24] designed a honing MR polishing apparatus. Multiple magnetic poles were arranged on a rotating shaft which could move back and forth, and the internal surface of different materials could be polished by using the stiffened MR polishing fluid. However, the disadvantage is that the embedded magnetic pole limits the diameter of the pipe that can be polished.

In the previous author's work [25], the horizontal MR polishing apparatus was designed to polish the internal surface of the titanium-alloy pipe. However, because of the horizontal structure of

 doi:10.20944/preprints202402.0423.v1

the MR polishing apparatus, the polishing particles in the MR polishing fluid will gradually deposit in the polishing area at the bottom of the pipe under the action of its gravity when the motor rotates at a high speed, resulting in different polishing areas with different concentrations of polishing particles. Moreover, when the MR polishing fluid flows out from the polishing head to the polishing area and accumulates to a certain extent in the polishing area, the excess MR polishing fluid flows out from both sides of the pipe so that the MR polishing fluid cannot be filled. Besides, the unsupported end face of the fixture is a cantilever structure, which causes excessive vibration and noise during the polishing process. Therefore, in this work, a new polishing method integrated with the apparatus of vertical magnetorheological polishing (VMRP) is introduced and implemented to achieve high surface performance. In order to validate the effectiveness of the proposed approach, the mechanisms of MR polishing of the internal surface of the titanium-alloy pipe are studied, followed by a series of experimental tests. In the experimental tests, the polishing performances are evaluated with respect to three different principal parameters: effect of the polishing time, effect of the particle size and effect of the rotation speed. Finally, the value of surface roughness due to each parameter is identified and corresponding surface topography is analyzed.

2. MR Honing Polishing Process

2.1. Polishing Mechanism

The MR honing polishing mechanism is illustrated in Figure 1. As shown in Figure 1, the material removal is obtained by the relative motion between polishing particles and the workpiece surface in the MR polishing process. The central part of the cross-section of the titanium-alloy pipe is the polishing head. The MR polishing fluid flows out of the polishing head and gets stiffened under the action of a magnetic field which is provided by a permanent magnetic field to form a "flexible polishing film". Then, the flexible polishing film is closely adhered to the surface of the polishing head, thickens with the continuous inflow of MR polishing fluid, and finally contacts with the internal surface of the pipe. Moreover, the flexible polishing film moves with the reciprocating movement of the polishing head, and the pipe maintains high-speed rotation. Thus, both axial and circumferential composite motions relative to the internal surface of the pipe are obtained.

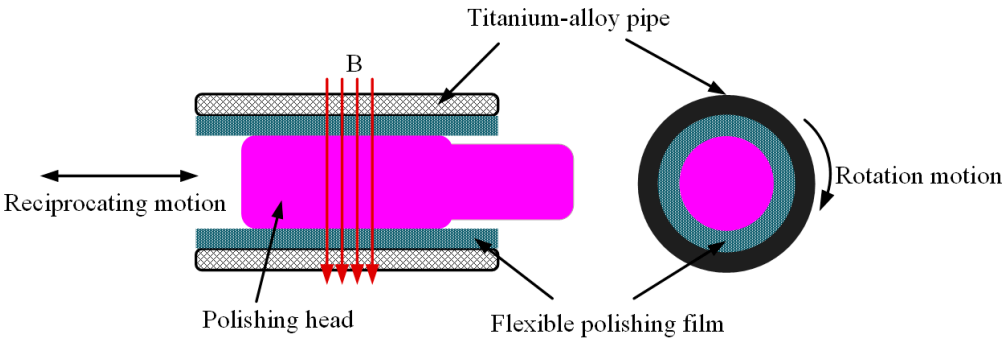

Figure 1. Schematic diagram of honing MR polishing principle.

The microcosmic distribution of MR fluid and MR polishing fluid is illustrated in Figure 2. The carbonyl iron powder (CIP) particles in MR fluid are distributed randomly, and MR fluid shows its flow characteristics and behaves no magnetism under a zero magnetic field. But under the magnetic field supplied by the excitation equipment, CIP particles from the MR fluid are polarized into magnetic dipoles [21]. Then, the adjacent magnetic dipoles will attract each other and arrange in order, forming an organized chain structure in the MR fluid. However, under a magnetic field, because the size of the polishing particles is larger than the size of CIP particles, the polishing particles will insert into the gap between the two adjacent CIP chains. The main function of abrasive particles is to remove surface material. This is because the soft CIP particles of the spherical shape have the

 doi:10.20944/preprints202402.0423.v1

much lower material removal rate compared with the abrasive particles in the MR polishing fluid [26]. In general, the shear performance of MR fluid in a magnetic field determines the scene of practical application. The yield stress provided by the MR fluid is the mechanical energy applied perpendicular to the direction of the CIP chain formation under a magnetic field, which is also the minimum stress value required at the beginning of the flow of MR fluid [27,28]. The yield stress is applied to the workpiece due to the rotation of flexible polishing film pushing the polishing particles to polish, and then the high-hardness polishing abrasive particles with irregular and sharp edges remove the metal surface material [29]. When CIP chains move relative to the internal surface of the titanium-pipe, the removal of surface material by the polishing particles embedded in the CIP chain is achieved. Under the repeated scraping of multiple polishing particles, the convex material on the workpiece surface is removed, and the workpiece surface roughness is decreased accordingly, and so the polishing effect is achieved.

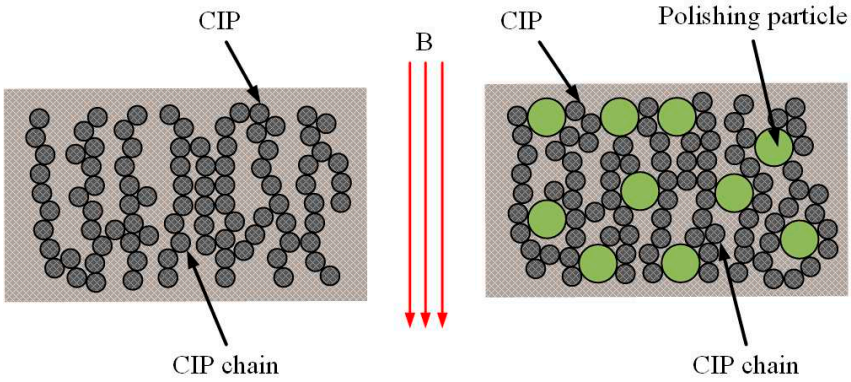

Figure 2. Chain structure of MR fluid and MR polishing fluid.

2.2. Design of the Polishing Apparatus

In this work, a new type of VMRP apparatus was designed to further improve the operation stability of the original apparatus to reduce the vibration and noise in the operation process, and hence improve the polishing performance. The VMRP apparatus and its circulation diagram of the MR polishing fluid are presented in Figure 3. The MR polishing fluid flows from the polishing shaft to the polishing head and flows out from the rectangular hole of the polishing head. A portion of MR polishing fluid gets stiffened under the action of the magnetic field and adheres to the polishing head. At the same time, the remaining MR polishing fluid enters the lower fixture and is thrown out of the rectangular hole by the high-speed rotating fixture. Then, it flows out of the hole at the bottom of the collecting groove and is finally collected and reused. Besides, by controlling the inflow and outflow speed of MR polishing fluid, the MR polishing fluid can maintain a relatively stable height in the pipe and the pipe rotates at a high speed. Then, the polishing head is inserted into the MR polishing fluid, which can make the MR polishing fluid in the pipe more uniformly and hence reduce the particle deposition.

 doi:10.20944/preprints202402.0423.v1

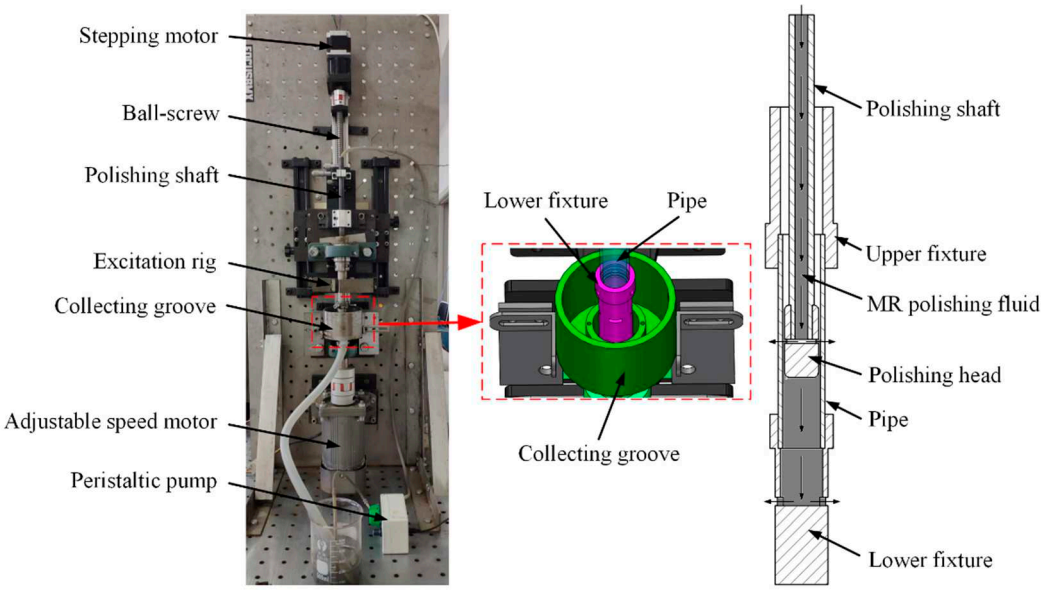

Figure 3. Photograph and schematic diagram of the VMRP apparatus.

2.3. Design and Simulation of the Magnetic Field

The magnetic field was provided by the permanent magnet, which was symmetrically arranged along the section of the titanium-alloy pipe to obtain multiple polishing areas. The diagram of the magnetic field assignment is shown in Figure 4. The arrangements of the permanent magnet were divided into two schemes. In scheme 1, the opposite poles had the same polarity, and in scheme 2, and the opposite poles had opposite polarity. To investigate the effect of different working gaps on the distribution of magnetic field and the magnetic field strength in the polishing area under different magnetic field arrangements, the simulation for the static magnetic field of the excitation device is carried out using Ansoft Maxwell finite element software. The working gap is the distance between the permanent magnet and the external surface of the titanium-alloy pipe, which is set as 1 mm to observe the distributions of the magnetic field.

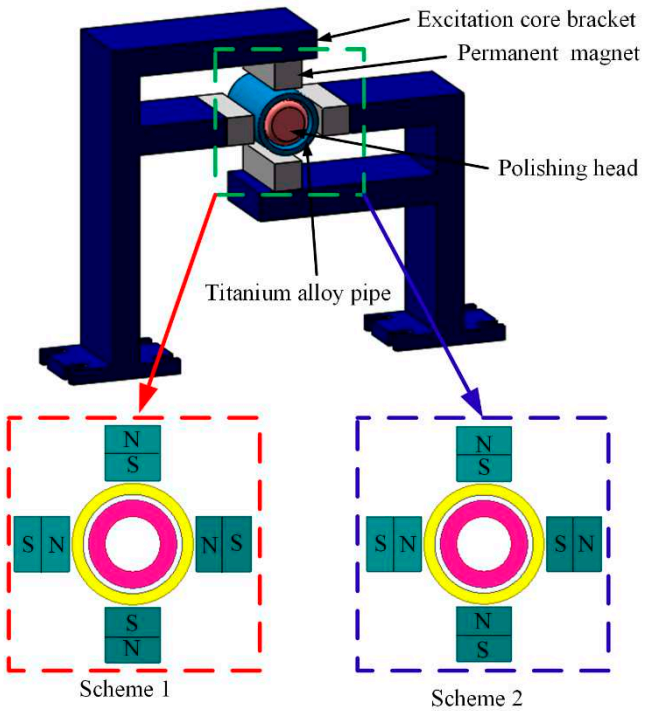

 doi:10.20944/preprints202402.0423.v1

Figure 4. Diagram of the magnetic field assignment.

The distributions of the magnetic flux under different assignments were shown in Figure 5. A closed gradient loop was formed inside the excitation core bracket in both schemes. However, outside the exciter core bracket, shown in Figure 5a, each adjacent permanent magnet formed a loop consisting of four closed loops in total; in Figure 5b, only the permanent magnets on the same exciter core bracket formed a loop, forming two closed loops in total. When a closed loop is formed between permanent magnets, theoretically, the polishing area increases with the loops increase. Therefore, the polishing area is larger under the opposite side with the same polarity. The magnetic field strength in different working gaps under different schemes is shown in Figure 6. With the increasing working gap, the magnetic flux density of the polishing area decreased gradually. In scheme 1, along with the directions of the magnetic field, the magnetic flux density between two adjacent permanent magnets increased firstly, then decreased and finally increased. Moreover, the maximum magnetic flux density of the polishing area decreased from 0.45T to 0.37T with the working gap increased from 0.5mm to 2mm, and the magnetic field distribution in the polishing area was relatively uniform. In scheme 2, along with the directions of the magnetic field, the magnetic flux density on the surface of the polishing head increased first and then decreased. Moreover, the maximum magnetic flux density of the polishing area decreased from 0.4T to 0.2T with the working gap increased from 0.5mm to 2mm. In practical polishing, there was a certain requirement for the magnitude of magnetic flux density. In scheme 1, the magnetic flux density of the polishing area was larger, and the proportion of the polishing area that satisfied the magnetic flux density was larger than scheme 2. In scheme 2, although only two closed loops were formed, the magnetic field strength in the polishing head area was stable, and the sensitivity to the working gap was small. In addition, the gradient magnetic field was formed. However, the larger magnetic field strength will lead to the magnetic particles in the MR polishing fluid completely adsorbed on the polishing head, and the MR polishing fluid in the polishing head cannot flow out. Besides, the polishing head was a kind of magnetic material, which would be affected under the action of the magnetic field. Therefore, scheme 1 was selected because four polishing areas formed, which will greatly improve the polishing efficiency, and the working gap of polishing is preferably 1 mm.

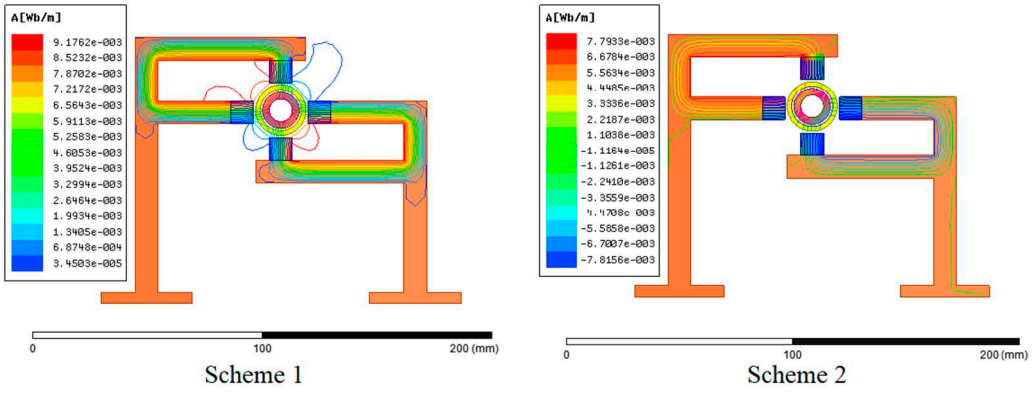

Figure 5. Distributions of the magnetic flux under different assignments.

Preprints.org (www.preprints.org) | NOT PEER-REVIEWED | Posted: 7 February 2024 doi:10.20944/preprints202402.0423.v1

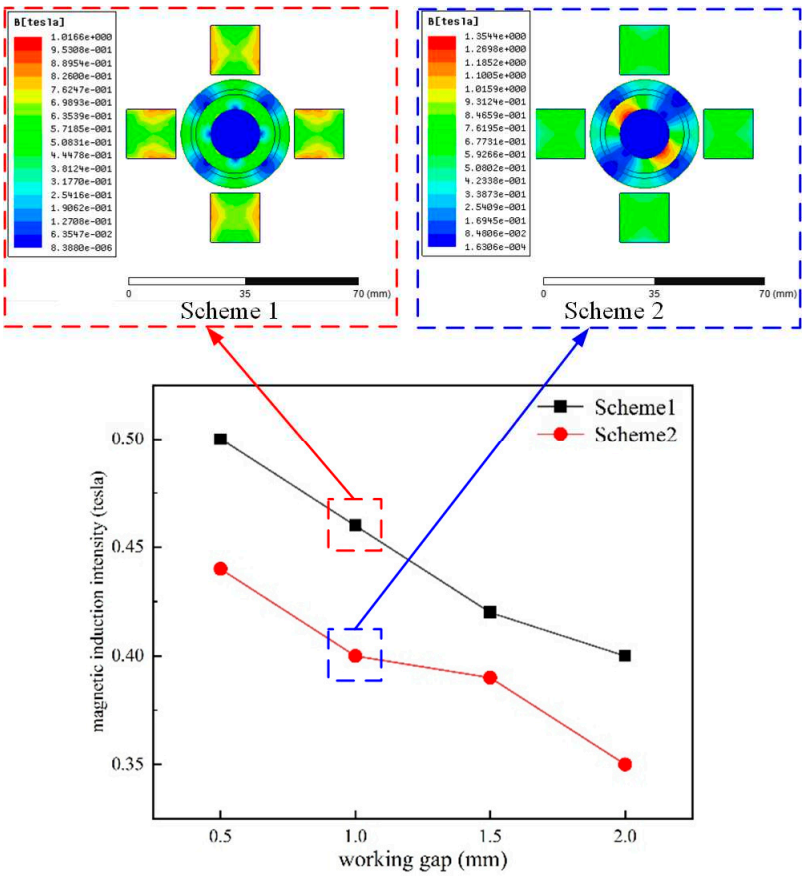

Figure 6. Simulation of the magnetic field strength in different working gaps for different schemes.

3. Experimental Methods

3.1. MR Polishing Fluid

The MR polishing fluid consists of the magnetic particles, abrasive particles, carrier liquid, and additives. The CIP is preferable as the magnetizable particle due to its high permeability and low magnetic remnant, and under the magnetic field, the CIP particles align in the magnetic field direction and form a chain structure [30]. The water-based carrier fluid is a preferable option for polishing metal surfaces, and the deionized water is selected as the carrier fluid because a hydrated layer can be formed on the workpiece surface [31]. Additives are added to MR polishing fluid to improve the suspension stability of MR polishing fluid. According to the previous research, the diamond abrasive particles with a volume fraction of 10% are more appropriate for polishing titanium-alloy pipes [25]. The specific volume fraction of each composition is presented in Table 1.

Table 1. The proportion of composition of MR polishing fluid.

Constituents of MR polishing fluid	Concentration (%)
Carbonyl iron powder	30
Diamond powder	10
Glycerol	8
Deionized water	52

3.2. Polishing Conditions

 doi:10.20944/preprints202402.0423.v1

The TA2 titanium alloy pipe is used as the workpiece to be polished, which has a length, external diameter, and internal diameter of 100 mm, 22 mm, and 18 mm, respectively. The production process was chosen as cold rolling and the outer surface was deburred and pickled. The sandpaper was used to grind axially along with the internal surface of the titanium-alloy pipe before polishing to realize the pretreatment of the pipe, which can remove the oxide layer, surface pits, and other defects on the internal surface and create a good condition for the subsequent MR finishing process. Moreover, for the same test of MR polishing experiments, the specimens with similar initial surface roughness were selected to reduce the deviation of the initial surface roughness. The internal surface of the pipe was polished partially to easily distinguish the polished areas and the unpolished areas. Besides, the polishing head is made of a ferromagnetic material, which can ensure that the flow of MR polishing fluid inside the polishing head is not affected by the external magnetic field [25]. The specific polishing conditions are presented in Table 2.

Table 2. Polishing conditions.

Parameter	Values
Polishing gap	1 mm
Reciprocating stroke	10 mm
Reciprocating linear speed	7.5 cycles per minutes
Feeding speed	2.5 mm/s

3.3. Experimental Design of the VMRP Process

MR polishing experiments are undertaken without and with the permanent magnetic field to evaluate the polishing performance and efficiency of MR polishing. The yield stress of MR polishing fluid depends on the strength of the magnetic field, the composition of the MR polishing fluid, the particle size, and the particle distribution [32]. Hence, the lower shear stress of MR polishing fluid can be overcome by changing the parameters of the polishing process. Moreover, the experiment is designed according to the method of the controlling of variable. Only one of the factors is changed each time, while the other factors are unchanged. By doing this, the influence of the changed factor on the polishing effect can be accurately evaluated. The MR polishing experiments under the VMRP apparatus are divided into 3 tests, and the total revolutions per test of the pipes are constant in each test. The experiments in Test 1 were conducted to study the effect of different polishing time on the polishing performance. According to the previous horizontal MR polishing experiments, the titanium-alloy pipe has the best polishing effect at 700 rpm, and the particle sizes of CIP and diamond powder were 18 μm and 20 μm, respectively [25]. Hence, the rotation speed of the pipe is chosen as 700 rpm, and the polishing time is set as 675, 1350, 2025, and 2700 cycles, respectively. Furthermore, the combined experiments of CIPs and polishing particles of different sizes in Test 2 are conducted at the same polishing time and rotation speed as in Test 1 to investigate the influence of different particle sizes only on the polishing performance. Finally, the combined experiments of different rotation speed in Test 3 are conducted at the same revolution and particle size as in Test 1 to investigate the influence of different rotation speeds on the polishing performance.

3.4. Measurement of Surface Roughness and Removal Mass

The variation of roughness and removal mass before and after polishing are found to assess the polishing performance. The electronic analytical balance is used to weigh the mass of material removal. The model of the OLS4100 3D laser microscope developed by Olympus Co. Ltd. is used to measure the variation of the surface roughness of the internal surface of the titanium-alloy pipe. The mass and roughness of pipes before and after polishing are then compared and corrected with the standard part prepared in advance. Moreover, the measurement before and after polishing of each test was carried out three times to take the average value to reduce the deviation.

4. Results and discussions

 doi:10.20944/preprints202402.0423.v1

4.1. Test 1: Effect of the Polishing Time on the Polishing Performance

Experiments to investigate the polishing performance using the VMRP apparatus were carried out after 675, 1350, 2025, and 2700 cycles, respectively. The settings of specific experimental parameters are given in Table 3. The internal surface and surface topography are shown in Figure 7. For the internal surface of the pipe, after 675 and 1350 cycles, the polished areas only had a metallic matte texture. After 2025 cycles, the polished area showed a specular metallic luster. After 2700 cycles, the surface finish of the polishing area was not significantly improved. For the surface topography, after 2025 cycles, the surface finish of the pipe is high. However, the deep initial axial scratches and slight removal traces of polishing particles were left on the surface of the pipe. After 2700 cycles, the depth of the remaining initial axial scratches further decreased, and the surface finish of the pipe had been greatly improved. However, the polished surface was mostly the removal traces of polishing particles cutting along the circumferential direction. The main reason that affected the surface finish has been changed from the initial scratches to the removal traces of polishing particles.

Table 3. Test 1: experiments with different polishing time.

Rotation speed (rpm)	Size of CIP and polishing particles (μm)	Polishing time (cycles)	Revolutions (r)
700	18 and 20	675	63000
		1350	126000
		2025	189000
		2700	252000

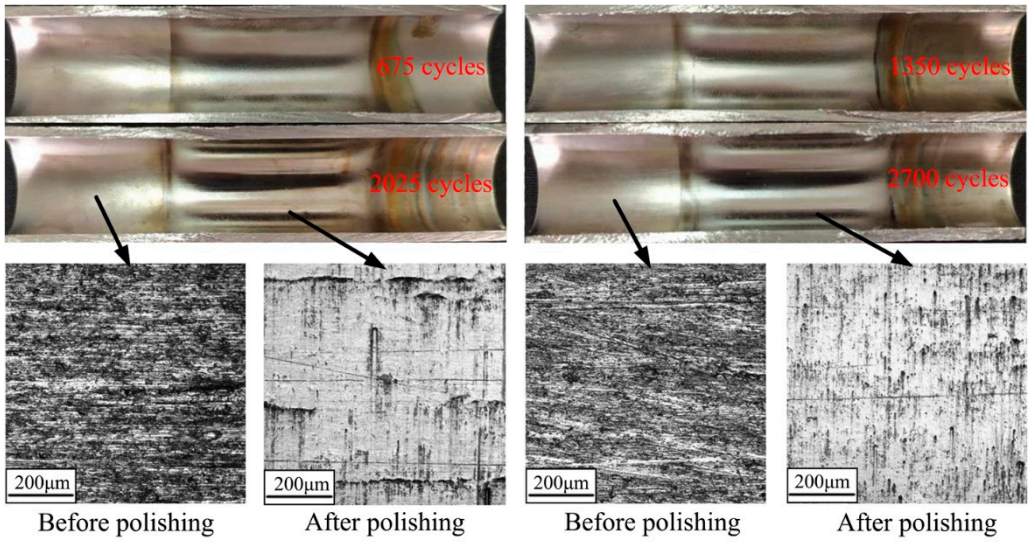

Figure 7. The internal surface and surface topography of pipes under different polishing time.

The axial surface roughness and circumferential surface roughness of pipes are shown in Figure 8. As shown in Figure 8a, the average initial axial surface roughness of the pipe is about 0.23 μm. When the polishing time was 675 cycles, 1350 cycles, 2025 cycles and 2700 cycles, the final axial surface roughness of the internal surface of the pipe was 0.112 μm, 0.093 μm, 0.079 μm and 0.081 μm, respectively. The final axial surface roughness of the pipe continues to decrease before reaching 2025 cycles, and it remains at a relatively stable value after 2700 cycles. In the early stage of polishing, the final axial surface roughness decreases rapidly. With the polishing time further increases, the material removal efficiency is reduced. This is because in the early stage of polishing, most of the tips of convex peaks on the internal surface of the workpiece are first removed by polishing particles, which makes the polishing efficiency faster. When polishing time is further increased, more material needs to be removed to smooth the remaining convex peaks and deep pits on the internal surface to decrease the surface roughness after the tips of convex peaks are removed. Moreover, the circumferential removal

 doi:10.20944/preprints202402.0423.v1

traces caused by the cutting movement of the polishing particles were left on the polished surface, and the final axial surface roughness was mainly determined by the circumferential removal traces. As shown in Figure 8b, the average initial circumferential surface roughness of the pipe is 0.3 μm. When the polishing time was 675 cycles, 1350 cycles, 2025 cycles and 2700 cycles, the final circumferential surface roughness of the internal surface of the pipe was 0.173 μm, 0.146 μm, 0.098 μm and 0.07 μm, respectively. When the polishing time gradually increases, the final circumferential surface roughness of the pipe continues to decrease. In the early stage of polishing, the tips of convex peaks on the workpiece surface are first removed, and the final circumferential surface roughness decreases rapidly. With increasing cycles, the depth of the axial scratches gradually decreased, and the final circumferential surface roughness was mainly determined by the depth of the axial scratches. After 2700 cycles, the final axial surface roughness is greater than the final circumferential surface roughness. The main reason is that the circumferential removal traces of polishing particles affected the axial surface roughness. Besides, both the variation of the surface roughness gradually increases with increasing cycles in Figure 8a,b. As the polishing time gradually increases, the amount of material removal on the surface of the workpiece also gradually increases. Therefore, under the similar initial surface roughness condition, the variation of the surface roughness gradually increases. The mass of material removal is shown in Figure 9. The mass of material removal increases with increasing revolutions, but the material removal rate increases first and then decreases. Because in the early stage of polishing, the convex peaks on the surface are removed rapidly, and in the later stage of polishing, removing the material on the polished surface is more difficult.

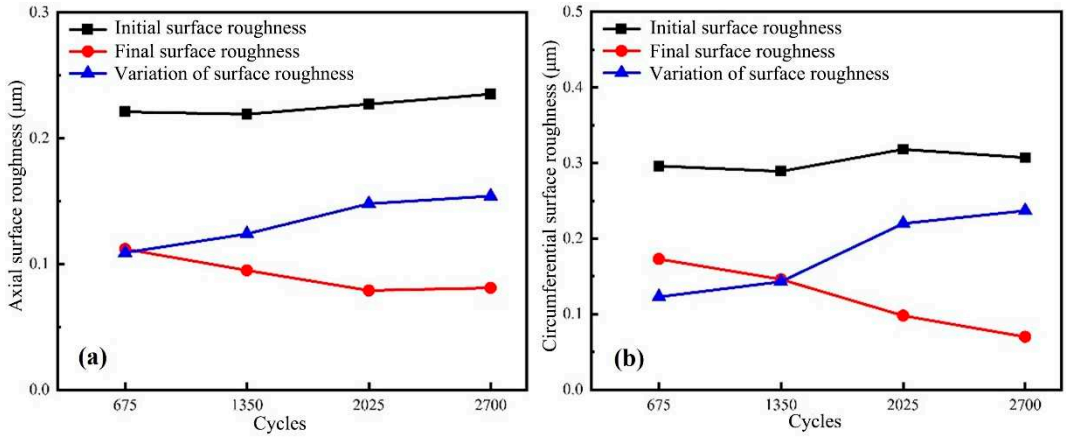

Figure 8. The axial surface roughness and circumferential surface roughness of pipes under different polishing time.

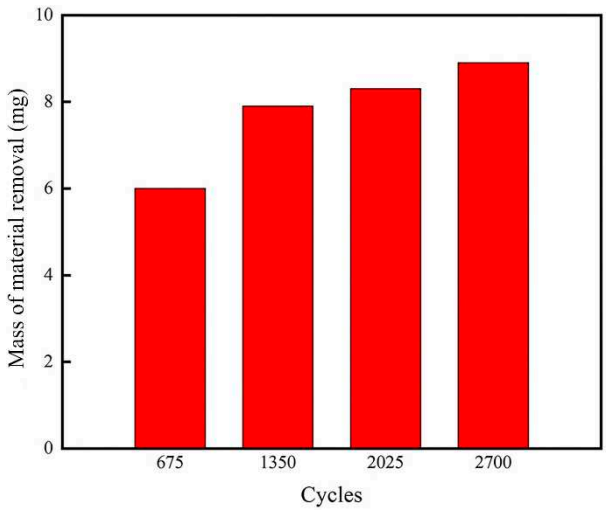

Figure 9. The mass of material removal of pipes under different polishing time.

 doi:10.20944/preprints202402.0423.v1

4.2. Test 2: Effect of the Particle Size on the Polishing Performance

Experiments to investigate the polishing performance under different size combinations of particles were conducted after 675, 1350, 2025, and 2700 cycles, respectively. The settings of specific experimental parameters are given in Table 4. The particle size combinations of CIP and polishing particles were 18 μm and 20 μm, 10 μm and 10 μm, 5 μm and 5μm, respectively. The internal surface and surface topography are shown in Figure 10. It can be seen from the internal surface of pipes that the polishing effect of the internal surface gradually improved with the continuous increase of the polishing time. After 675 cycles, the polished area with different size combinations of particles get a metallic luster. Moreover, the metallic luster was more significant with increasing cycles, and the polishing effect reached the best after 2700 cycles. Compared with the Test 1 with the particles of a single size, the introduction of a combination of smaller CIP and polishing particles further improved the removal traces caused by the original polishing particles of a single size, and the surface finish of the pipe has been significantly improved. Besides, it can be seen from the surface topography of pipes that compared with Test 1, the depth of initial axial scratches significantly decreased after 2025 cycles, and the circumferential removal traces were more uniform. This is because smaller polishing particles not only decreased the depth of initial scratches by removing the surface material but also improved the removal traces of larger polishing particles. However, some circumferential removal traces were left on the surface, which was caused by the insufficient material removal of small polishing particles. After 2700 cycles, the surface finish was greatly improved and the depth of initial axial scratches further decreased, and only a few removal traces were left on the polished surface. The axial surface roughness and circumferential surface roughness of pipes are presented in Figure 11. The average initial axial and circumferential surface roughness of the pipes were approximately 0.25 μm and 0.36 μm, respectively, which was close to the initial surface roughness of Test 1. When the polishing time were 675 cycles, 1350 cycles, 2025 cycles and 2700 cycles, the final axial surface roughness of the pipes were 0.132 μm, 0.094 μm, 0.071 μm and 0.05 μm, respectively, and the final circumferential surface roughness of the pipes were 0.206 μm, 0.096 μm, 0.061 μm and 0.038 μm, respectively. It can be seen that when the polishing time gradually increased, the final axial and circumferential surface roughness of the pipe continue to decreased. Moreover, the axial and circumferential surface roughness were lower than that in Test 1 for longer polishing time. It is known that the larger polishing particles dominated the removing of the tips of convex peaks on the workpiece surface in the early stage of polishing process, so it could effectively remove the forming marks on the inner surface of the pipe with increasing polishing time, then the smaller polishing particles could significantly remove the polishing traces introduced by the larger polishing particles. Incidentally, the initial surface roughness of the pipe was low under 2700 cycles, and the polishing effect of larger particles was not very obvious, and thus the variation of the surface roughness showed a decreasing trend. While the removal effect of smaller particles was more significant, the axial and circumferential surface roughness was still smaller. The mass of material removal is shown in Figure 12. It is observed that the total material removal gradually increased with increasing polishing time, which is consistent with the change in surface roughness. With the removal of surface protrusions and surface materials, the relative depth of scratches and the pits gradually decreased, and the surface roughness also continues to be decreased.

Table 4. Test 2: experiments with different particle sizes.

Rotation speed (rpm)	The polishing time under different sizes of particles (cycles)			Revolutions (r)
	18 μm and 20	10 μm and 10 μm	5 μm and 5 μm	
700	225	225	225	63000
	450	450	450	126000
	675	675	675	189000
	900	900	900	252000

 doi:10.20944/preprints202402.0423.v1

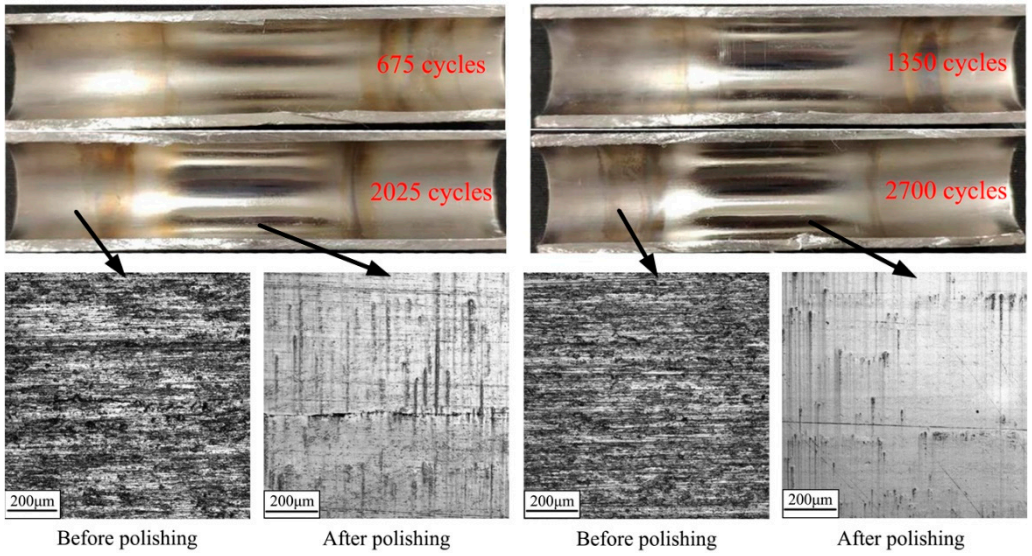

Figure 10. The internal surface and surface topography of pipes under different size combinations of particles.

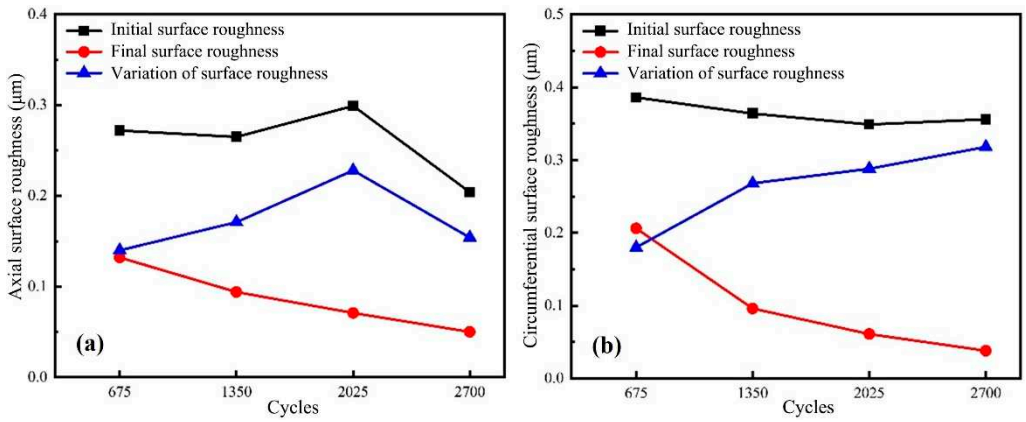

Figure 11. The axial surface roughness and circumferential surface roughness of pipes under different size combinations of particles.

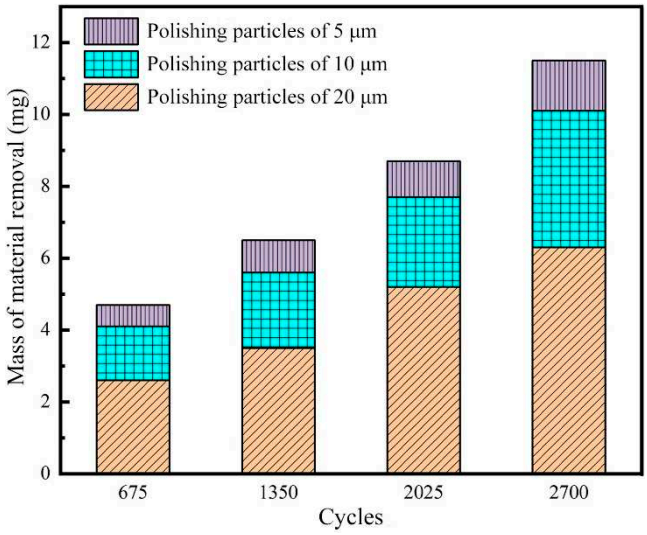

Figure 12. The mass of material removal of pipes under different size combinations of particles.

 doi:10.20944/preprints202402.0423.v1

4.3. Test 3: Effect of the Rotation Speed on the Polishing Performance

Experiments to investigate the polishing performance are conducted under different rotation speed of 1120 r/min, 980 r/min, 840 r/min, 700 r/min, respectively. The settings of specific experimental parameters are given in Table 5. Because of the increase of the rotation speed in Test 3, the same revolutions can be obtained with less polishing time, and the total revolutions of Test 3 in each rotation speed combination should be consistent with Test 1 and Test 2. The internal surface and surface topography are shown in Figure 13. For the internal surface of pipes, the polishing effect of the pipe polished is not much different in test 1 and test 3. The internal surface of the pipe polished in Test 3 already had a metallic specular effect for 126000 revolutions, while the pipe polished in Test 1 only had a metallic matte texture. After 189000 revolutions, although the polished pipe had a metallic specular effect in Test 1 and 3, the polishing effect of the pipe was better in Test 3, and the polishing time was shorter. For the surface topography, the original shallow axial scratches have been completely removed after 126000 revolutions in Test 3, and the deeper axial scratches gradually became shallow and only the slight material removal traces are left by the polishing particles. Compared with the surface topography of the pipe polished in Test 1 after 252000 revolutions, the pipe polished in Test 3 was polished to the better degree with only 126000 revolutions, which greatly shortens the polishing time and improves the polishing efficiency. However, the surface topography polished in Test 3 after 252000 revolutions is the worst. This is because of the excessive removal of polishing particles damage the polishing surface. Moreover, a lots of removal traces are left on the workpiece surface by the large polishing particles in the later stage of polishing under the polishing of higher rotation speed.

Table 5. Test 3: experiments with different rotation speeds.

CIP and polishing particles (μm)	The polishing time under different rotation speeds (cycles)				Revolutions (r)
	1120 rpm	980 rpm	840 rpm	700 rpm	
18 and 20	105	120	140	169	63000
	210	240	280	338	126000
	315	360	420	507	189000
	420	480	560	676	252000

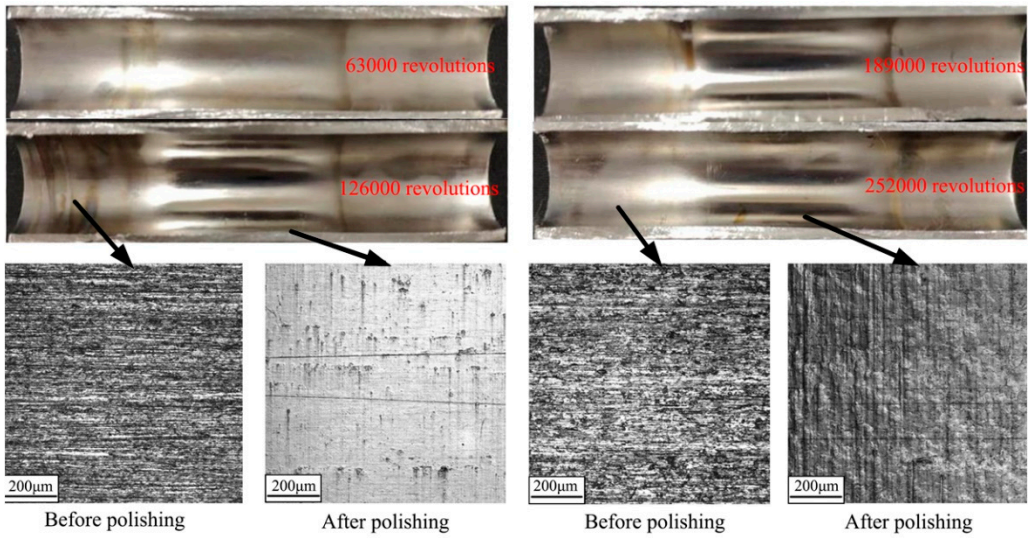

Figure 13. The internal surface and surface topography of pipes under rotation speed combinations.

 doi:10.20944/preprints202402.0423.v1

The axial surface roughness and circumferential surface roughness are presented in Figure 14. The average initial axial and circumferential surface roughness of the pipe were approximately 0.24 μm and 0.31 μm, respectively, which was close to the initial surface roughness of Test 1. When the revolutions were 63000, 126000, 189000 and 252000, the final axial surface roughness of the pipe were 0.121 μm, 0.084 μm, 0.04 μm and 0.129 μm, respectively, and the final circumferential surface roughness of the pipe were 0.174 μm, 0.066 μm, 0.045 μm and 0.109 μm, respectively. It is observed that when the polishing time gradually increased, the final axial and circumferential surface roughness of the pipe decreased rapidly to a minimum value, but increased after 252000 revolutions. After 63000 revolutions, the final axial and circumferential surface roughness polished in Test 3 was close to the surface roughness polished in Test 1. After 126000 and 189000 revolutions, the final axial and circumferential surface roughness of the pipes polished in Test 3 decreased to a lower value compared with the pipe polished in Test 1. This attributed to the material removal, and hence increased with the increasing rotation speed of the pipe in unit time. However, the final axial and circumferential surface roughness of the tubes in Test 3 significantly increased for 252000 revolutions. This phenomenon is explained by the fact that the precision polishing ability of the MR polishing fluid significantly decreased as the temperature of the polishing area increased under long-term high-speed rotation conditions, and the complex wear phenomena occurred in the polishing area. From Figure 13, it is also seen that the circumferential wear marks left on the polished surface were extremely dense, which becomes the main factor affecting the axial and circumferential surface roughness, and this is consistent with the trend of surface roughness variation shown in Figure 14. The mass of material removal is shown in Figure 15. It is identified from this result that the polishing process achieved the better material removal under the combined rotational speed, and the removal amount gradually increased with the increase of revolutions. In the early stage of polishing, the surface protrusions could be easily removed under the higher motor speed and the removal amount also gradually increased; In the later stage of polishing, the inner surface of the pipe was relatively flat, and the material removal was relatively difficult for relying on polishing particles to press into the polished surface. Meanwhile, the motor speed was low, and the amount of material removal decreased accordingly. The combined polishing process using multiple motor rotation speeds greatly improves polishing efficiency. Moreover, compared with the polishing effect polished in Test 1 after 2700 cycles, it is calculated that the combination of different rotation speeds can achieve the same or even better polishing effect after 1602 cycles under the same revolutions. In short, the optimal axial surface roughness of 0.04 μm for the polished inner surface using VMRP approach in this study. It is here noted that axial surface roughness using the horizontal MR polishing apparatus was identified of 0.401 μm [25], which is much larger than the value obtained in this work. In addition, it has been found that although the initial surface roughness of the pipes is different for in the two types of apparatus, there is a significant improvement in the changes of surface roughness from 47.85% to 83.34%. demonstrating the better polishing efficiency in MR polishing technology.

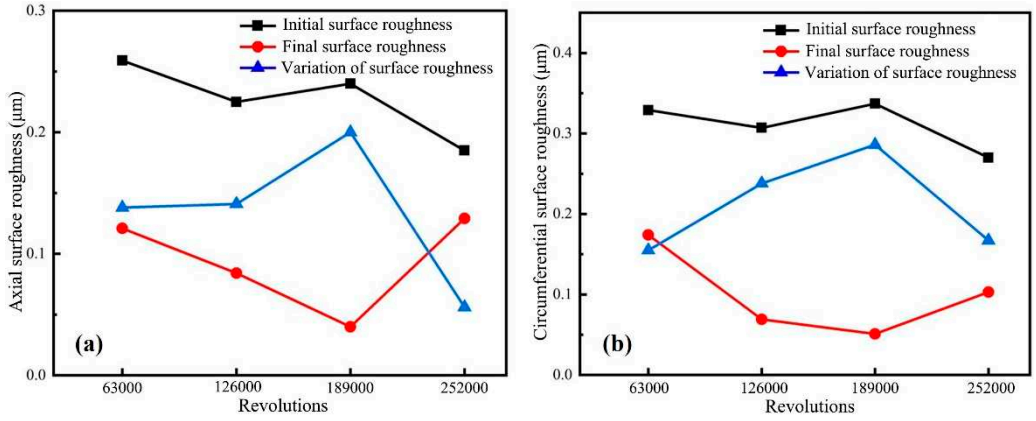

Figure 14. The axial surface roughness and circumferential surface roughness of pipes under rotation speed combinations.

 doi:10.20944/preprints202402.0423.v1

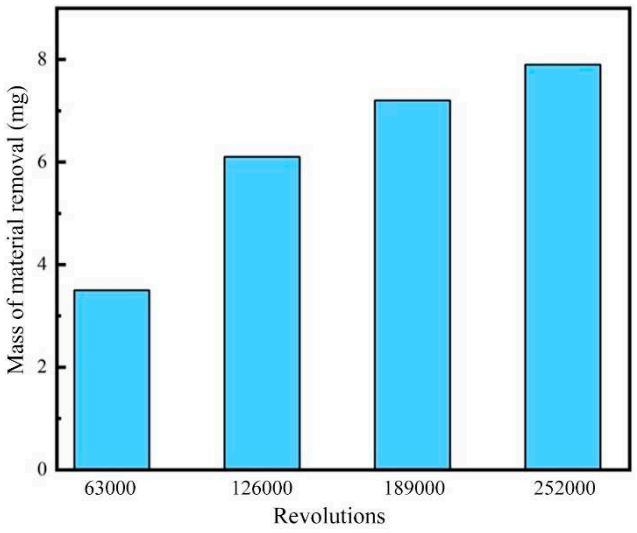

Figure 15. The mass of material removal of pipes under rotation speed combinations.

5. Conclusions

In this paper, the VMRP apparatus were designed to overcome the structural limitation of the previous horizontal MR polishing apparatus, and hence improve the polishing performance further. The main technical results achieved from this experimental work are summarized as follows: (i) A vertical MR polishing method is formulated based on the principle of MR polishing and experimentally realized to improve surface efficiency by reducing unwanted vibration and noise during operation compared to the previous horizontal MR polishing apparatus. (ii) By using finite element software to simulate and analyze the magnetic field of the excitation rig, it was found that the permanent magnet with circumferential distribution can form four magnetic induction line circuits under the opposite polarity arrangement scheme, and the polishing area becomes larger and the magnetic field strength meets the polishing requirements. (iii) The influence of particle combination and rotational speed combination on the MR polishing effect was studied in the vertical MR polishing process, and the polishing mechanism was revealed under different CIP and polishing particle combinations. The experiment results obtained from proposed polishing VMRP apparatus show the nanoscale polishing surface quality of 0.04 μm, while the horizontal polishing apparatus gives 0.401 mm.

Consequently, this study verifies the feasibility of VMRP polishing process, and provides high quality and efficiency of MR polishing for the inner surface of the pipe. However, the optimal polishing surface quality and polishing efficiency of MR polishing technology will be systematically investigated under the coupling effect of magnetic field strength, particle combination and speed combination need to be explored more in future. Furthermore, the theoretical or analytical constitutive model associated with experimental coefficients, which can predict the polishing performance, is required to be formulated using deep learning, neural network, fuzzy technique and algorithms to enhance polishing technology using MR fluids.

Author Contributions: Conceptualization, W.L.S., N.W. and S.-B.C.; methodology, W.L.S. and S.-B.C.; validation, W.L.S., Z.Y. and D.Z.M.; formal analysis, W.L.S. and S.-B.C.; investigation, W.L.S., N.W. and S.-B.C.; resources, W.L.S., N.W. and S.-B.C.; data curation, W.L.S., Z.Y. and D.Z.M.; writing—original draft preparation, W.L.S., Z.Y., D.Z.M. and S.-B.C.; writing—review and editing, W.L.S. and S.-B.C.; visualization, W.L.S. and S.-B.C.; supervision, W.L.S.; project administration, W.L.S.

Funding: Please add: This project was supported by the National Natural Science Foundation of China (Grant No. 52005085).

Data Availability Statement: The data used to support the findings of this study are included in the manuscript.

Conflicts of Interest: The authors declare no conflict of interest.

References

1. Cui, C.X.; Hu, B.M.; Zhao, L.C.; Liu, S.J. Titanium alloy production technology, market prospects and industry development. *Mater. Des.* **2011**, *32*, 1684-1691.
2. Pervukhin, L.B.; Kryukov, D.B.; Krivenkov, A.O.; Chugunov, S.N. Structural transformations and properties of titanium–aluminum composite during heat treatment. *Phys. Metals Metallogr.* **2017**, *118*, 759-763.
3. Gao, P.F.; Fu, M.W.; Zhan, M.; Lei, Z.N.; Li, Y.X. Deformation behavior and microstructure evolution of titanium alloys with lamellar microstructure in hot working process: A review. *J. Mater. Sci. Technol.* **2019**, *39*, 56-73.
4. Karkalos, N.E.; Galanis, N.I.; Markopoulos, A.P. Surface roughness prediction for the milling of Ti–6Al–4V ELI alloy with the use of statistical and soft computing techniques. *Measurement* **2016**, *90*, 25-35.
5. Pervaiz, S.; Rashid, A.; Deiab, I.; Nicolescu, M. Influence of tool materials on machinability of titanium- and nickel- based alloys: A review. *Mater. Manuf. Process.* **2014**, *29*, 219-252.
6. Jain, V.K. Abrasive-based nano-finishing techniques: An overview. *Mach. Sci. Technol.* **2008**, *12*, 257-294.
7. Sidpara, A.; Jain, V.K. Analysis of forces on the freeform surface in magnetorheological fluid based finishing process. *Int. J. Mach. Tools Manuf.* **2013**, *69*, 1-10.
8. Nie, M.; Cao, J.G.; Li, J.Y.; Fu, M.H. Magnet arrangements in a magnetic field generator for magnetorheological finishing. *Int. J. Mech. Sci.* **2019**, *161*, 105018.
9. Grover, V.; Singh, A.K. Modelling of surface roughness in a new magnetorheological honing process for internal finishing of cylindrical workpieces. *Int. J. Mech. Sci.* **2018**, *144*, 679-695.
10. Tani, Y.; Kawata, K.; Nakayama, K. Development of high-efficient fine finishing process using magnetic fluid. *CIRP Ann.* **1984**, *33*, 217-220.
11. Kordonski, W.I.; Jacobs, S.D. Magnetorheological finishing. *Int. J. Mod. Phys. B* **1996**, *10*, 2837-2848.
12. Golini, D.; Kordonski, W.I.; Dumas, P. Magnetorheological finishing (MRF) in commercial precision optics manufacturing. *Opt. Manuf. Test III* **1999**, *3782*, 80-91.
13. Saraswathamma, K.; Jha, S.; Rao, P.V. Rheological characterization of MR polishing fluid used for silicon polishing in BEMRF process. *Mater. Manuf. Process.* **2015**, *30*, 661-668.
14. Singh, A.K.; Jha, S.; Pandey, P.M. Design and development of nanofinishing process for 3D surfaces using ball end MR finishing tool. *Int. J. Mach. Tools Manuf.* **2011**, *51*, 142-151.
15. Singh, A.K., S. Jha, and P.M. Pandey, Nanofinishing of a typical 3D ferromagnetic workpiece using ball end magnetorheological finishing process. *Int. J. Mach. Tools Manuf.* **2012**, *63*, 21-31.
16. Jung, B.; Jang, K.I.; Min, B.K.; Lee, S.J.; Seok, J. Magnetorheological finishing process for hard materials using sintered iron-CNT compound abrasives. *Int. J. Mach. Tools Manuf.* **2009**, *49*, 407-418.
17. Barman, A.; Das, M. Nano-finishing of bio-titanium alloy to generate different surface morphologies by changing magnetorheological polishing fluid compositions. *Precis. Eng.-J. Int.Soc. Precis. Eng. Nanotechnol.* **2018**, *51*, 145-152.
18. Gupta, K.; Laubscher, R.F. Sustainable machining of titanium alloys: A critical review. *Proc. Inst. Mech. Eng. Part B-J. Eng. Manuf.* **2017**, *231*, 2543-2560.
19. Kumar, R.; Roy, S.; Gunjan, P.; Sahoo, A.; Sarkar, D.D.; Das, R.K. Analysis of MRR and surface roughness in machining Ti-6Al-4V ELI titanium aAlloy using EDM process. *Procedia Manuf.* **2018**, *20*, 358-364.
20. Wang, Y.; Hu D.J.; Deng, Q.L. Study on internal magnetic abrasive finishing of thin and long austenitic stainless steel tube. *Key Eng. Mater.* **2004**, *259-2*, 620-625.
21. Zou, Y.H.; Shinmura, A.T. A New internal magnetic field assisted machining process using a magnetic machining jig-machining characteristics of inside finishing of a SUS304 stainless steel tube. *Ultra-precis. Mach. Technol.* **2009**, *69-70*, 143-147.
22. Kang, J.M.; George A.; Yamaguchi, H. High-speed internal finishing of capillary tubes by magnetic abrasive finishing. *Fifth CIRP Conference on high Performance Cutting 2012* **2012**, *1*, 414-418.
23. Sadiq, A.;Shunmugam, M.S. A novel method to improve finish on non-magnetic surfaces in magneto-rheological abrasive honing process. *Tribol. Int.* **2010**, *43*, 1122-1126.
24. Grover, V.; Singh, A.K. A novel magnetorheological honing process for nano-finishing of variable cylindrical internal surfaces. *Mater. Manuf. Process.* **2017**, *32*, 573-580.
25. Song, W.L.; Peng Z.; Li, P.F.; Shi, P.; Choi, S.B. Annular surface micromachining of titanium tubes using a magnetorheological polishing technique. *Micromachines* **2020**, *11*, 314.

 doi:10.20944/preprints202402.0423.v1

26. Shorey, A.B.; Jacobs, S.D.; Kordonski, W.I.; Gans, R.F. Experiments and observations regarding the mechanisms of glass removal in magnetorheological finishing. *Appl. Optics* **2001**, *40*, 20-33.
27. Yang, J.; Yan, H.; Wang, X.M.; Hu, Z.D. Enhanced yield stress of magnetorheological fluids with dimer acid. *Mater. Lett.* **2016**, *167*, 27-29.
28. Saraswathamma, K.; Jha, S.; Rao P.V. Rheological behaviour of magnetorheological polishing fluid for Si polishing. *Mater. Today-Proc.* **2017**, *4*, 1478-1491.
29. Mutalib, N.A.; Ismail, I.; Soffie, S.M.; Aqida, S.N. Magnetorheological finishing on metal surface: A review. *IPCME2018* **2019**, *469*, 012092.
30. Rahim, M.S.A.; Ismail, I. Review of magnetorheological fluids and nanofluids thermal behaviour. *ICMER 2015* **2015**, *100*, 012040.
31. Sidpara, A.; Jain, V.K. Effect of fluid composition on nanofinishing of single-crystal silicon by magnetic field-assisted finishing process. *Int. J. Adv. Manuf. Technol.* **2011**, *55*, 243-252.
32. Elizabeth Premalatha, S.; Chokkalingam, R.; Mahendran, M. Magneto Mechanical Properties of Iron Based MR Fluids. *Am. J. Polym. Sci.* **2012**, *2*, 50-55.